Does afforestation deteriorate haze pollution in Beijing–Tianjin–Hebei (BTH), China?

Xin Long[1, 3], Naifang Bei[2], Jiarui Wu[1], Xia Li[1], Tian Feng[1], Li Xing[1], Shuyu Zhao[1], Junji Cao[1], Xuexi Tie[1, 4], Zhisheng An[1], and Guohui Li[1*]

[1]Key Lab of Aerosol Chemistry & Physics, SKLLQG, Institute of Earth Environment, Chinese Academy of Sciences, Xi'an, 710061, China
[2]Institute of Global Environmental Change, Xi'an Jiaotong University, Xi'an, 710049, China
[3]Joint Center for Global Change Studies (JCGCS), Beijing 100875, China
[4]National Center for Atmospheric Research, Boulder, CO, 80303, USA

[*]Correspondence to: Guohui Li (ligh@ieecas.cn)

Abstract: Although aggressive emission control strategies have been implemented recently in the Beijing-Tianjin-Hebei area (BTH), China, pervasive and persistent haze still frequently engulfs the region during wintertime. Afforestation in BTH, primarily concentrated in the Taihang and Yanshan Mountains, has constituted one of the controversial factors exacerbating the haze pollution due to its slowdown of the surface wind speed. We report here an increasing trend of forest cover in BTH during 2001-2013 based on long-term satellite measurements and the impact of the afforestation on the fine particles ($PM_{2.5}$) level. Simulations using the Weather Research and Forecast model with chemistry reveal that the afforestation in BTH since 2001 generally deteriorates the haze pollution in BTH to some degree, enhancing $PM_{2.5}$ concentrations by up to 6% on average. Complete afforestation or deforestation in the Taihang and Yanshan Mountains would increase or decrease the $PM_{2.5}$ level within 15% in BTH. Our model results also suggest that implementing a large ventilation corridor system would not be effective or beneficial to mitigate the haze pollution in Beijing.

1 Introduction

Heavy haze with extremely high levels of fine particles ($PM_{2.5}$), caused by rapid growth of industrialization, urbanization, and transportation, frequently covers Northern China during wintertime, particularly in the Beijing–Tianjin–Hebei area (BTH). The haze pollution in BTH remarkably impairs visibility and potentially causes severe health defects (Lim et al., 2013; Wang and Hao, 2012). The Chinese State Council has issued the 'Air Pollution Prevention and Control Action Plan' (APPCAP) in September 2013 with the aim of improving China's air quality within five years and reducing $PM_{2.5}$ by up to 25% by 2017 relative to 2012 levels. Although aggressive emission control strategies have been undertaken since the initiation and implementation of the Action Plan, widespread and persistent haze still often engulfs BTH.

Aside from emissions, meteorological conditions play a key role in the haze pollution, affecting the formation, transformation, diffusion, transport, and removal of $PM_{2.5}$ in the atmosphere (Bei et al., 2012; 2017). Multifarious measurements have provided cumulative evidence that the widespread slowdown of surface wind speeds has occurred globally and in China since 1980s (Chen et al., 2013; McVicar et al., 2012), which facilitates the pollutant accumulation to deteriorate air quality (Zhao et al., 2013; Sun et al., 2016). An increase in the surface roughness induced by increased vegetative biomass has been proposed to be responsible for the surface-level stilling to some degree (Wu et al., 2016b; Vautard et al., 2010). Consequently, a debate has been circulated in China on whether the afforestation program contributes importantly to the haze formation in BTH (China foresty network, 2016a, 2017).

Deforestation and its potentials to severe droughts and massive floods raised serious concerns in China since 1970s, fostering the largest afforestation project in the world (Liu et al., 2008). Six key afforestation programs have been implemented since 2001 and "the Green

Great Wall" of China has been established in Northern China (Duan et al., 2011). A remarkable forest growth has been reported in the northwest of BTH from 2000 to 2010 (Li et al., 2016), which has the potential to increase the surface roughness and decrease the surface wind speed (Wu et al., 2016a; Bichet et al., 2012), and could potentially aggravate the haze pollution. In addition, previous studies have shown that the afforestation is beneficial for the atmosphere to remove O_3, NO_x, SO_2, and $PM_{2.5}$ through the dry deposition process (Zhang et al., 2015; 2017; Huang et al., 2016). Hence, a large artificial ventilation corridor system has been proposed, highly anticipated to ventilate Beijing (China forestry network, 2014, 2016b, c).

In the present study, we report an analysis of long-term satellite measurements of the land cover change in BTH and quantitatively evaluate the impacts of the afforestation on the haze pollution in BTH using the WRF-CHEM model. We have further evaluated the effect of the proposed large artificial ventilation corridor system on the haze mitigation in Beijing. The model configuration and methodology are provided in Section 2. Data analysis and model results are presented in Section 3, and conclusions are given in Section 4.

2 Data, model and methodology

2.1 MODIS data

The data utilized in the study are the annual land cover product, MCD12Q1, derived from the Terra- and Aqua- Moderate Resolution Imaging Spectroradiometer (MODIS) observations since 2001 (Friedl et al., 2002). The product has been widely used in studies of atmospheric science, hydrology, ecology, and land change science (Gerten et al., 2004; Guenther, 2006; Reichstein et al., 2007; Turner et al., 2007). Wu et al., (2008) have compared four global land cover datasets across China, concluding that the MODIS land cover product is the most representative over China with the minimal bias from the China's National Land

Cover Dataset. The MCD12Q1 (Version 5.1) IGBP (International Geosphere Biosphere Programme) scheme with a spatial resolution of 500 m is utilized to explore the variability of the land cover fraction (LCF) from 2001 to 2013 in BTH and assimilated into the WRF-CHEM model. The high-resolution land cover product is generated using a supervised classification algorithm in conjunction with a revised database of high quality land cover training sites (Friedl et al., 2002). The accuracy of the IGBP layer of MCD12Q1 is estimated to be 72.3-77.4% globally, with a 95% confidence interval on the estimate of 72.3-77.4% (Friedl et al., 2002; Friedl et al., 2010). Great efforts have been made to evaluate the accuracies of the global land cover datasets over China. The overall accuracy of MCD12Q1 in China is estimated to be 55.9-68.9% (Bai et al., 2015; Yang et al., 2017), which could be increased to about 70% when ignoring the differences of five forests.

2.2 WRF-CHEM model and configurations

We use a specific version of the WRF-CHEM model (Grell et al., 2005) to investigate the impacts of the afforestation on the haze pollution in BTH. The model includes a new flexible gas phase chemical module and the CMAQ/Models3 aerosol module developed by US EPA (Binkowski and Roselle, 2003). The wet deposition of chemical species follows the CMAQ method. The dry deposition parameterization follows Wesely (Wesely, 1989), and the dry deposition velocitiy of aerosols and trace gases is calculated as a function of the local meteorology and land use. The photolysis rates are calculated by FTUV (Fast Radiation Transfer Model) (Li et al., 2005). The inorganic aerosols are predicted using ISORROPIA Version 1.7 (http://nenes.eas.gatech.edu/ISORROPIA/) (Nenes et al., 1998). The secondary organic aerosol (SOA) is predicted using a non-traditional SOA module, including the VBS (volatility basis-set) modeling approach and SOA contributions from glyoxal and methylglyoxal. Detailed information about the WRF-CHEM model can be found in previous studies (Li et al., 2010; Li et al., 2011a, b; Li et al., 2012).

High $PM_{2.5}$ pollution episodes from 1 December 2013 to 31 January 2014 in the North China Plain (NCP) have been simulated using the WRF-CHEM model. The model simulation domain is shown in Figure 1, and detailed model configurations can be found in Table 1. The chemical initial and boundary conditions are interpolated from the 6h output of MOZART-4 (Emmons et al., 2010; Horowitz et al., 2013). MOZART-4 is driven by meteorology fields from the NASA GMAO GEOS-5 model, using anthropogenic emissions based on David Streets' inventory (Streets et al., 2006) and fire emissions from FINN-v1 (Widinmyer et al., 2011). The model has been evaluated comprehensively with several sets of observations, reproducing well tropospheric chemical composition (Emmons et al., 2010). The model results have been successfully and widely used as the initial and lateral boundary conditions for chemical transport models. The anthropogenic emission inventory used in the present study is developed by Zhang et al. (2009), with the base year of 2013, including contributions from agriculture, industry, power, residential and transportation sources. Figure S1 shows the emission distribution of OC, VOCs, NO_x, and SO_2 in the simulation domain. The high emissions of OC, VOCs, NOx, and SO_2 are generally concentrated in the plain region of BTH and Shandong province, the downwind area of afforestation.

The hourly near-surface CO, SO_2, NO_2, O_3, and $PM_{2.5}$ mass concentrations released by the China's Ministry of Environmental Protection are used to validate the model simulations and accessible from the website http://www.aqistudy.cn/.

We use the normalized mean bias (*NMB*), the index of agreement (*IOA*), and the correlation coefficient (*R*) to assess the WRF-CHEM model performance in simulating air pollutants against measurements.

$$NMB = \frac{\sum_{i=1}^{N}(P_i - O_i)}{\sum_{i=1}^{N} O_i} \quad (1)$$

$$IOA = 1 - \frac{\sum_{i=1}^{N}(P_i - O_i)^2}{\sum_{i=1}^{N}(|P_i - \bar{O}| + |O_i - \bar{O}|)^2} \quad (2)$$

$$R = \frac{\sum_{i=1}^{N}(P_i-\bar{P})(O_i-\bar{O})}{[\sum_{i=1}^{N}(P_i-\bar{P})^2 \sum_{i=1}^{N}(O_i-\bar{O})^2]^{\frac{1}{2}}} \quad (3)$$

Where P_i and O_i are the calculated and observed air pollutant concentrations, respectively. *N* is the total number of the predictions used for comparisons, and $\bar{P}$ and $\bar{O}$ represent the average of predictions and observations, respectively. The *IOA* ranges from 0 to 1, with 1 showing perfect agreement of the prediction with the observation. The *R* ranges from -1 to 1, with 1 implicating perfect spatial consistency of observations and predictions.

2.3 MCD12Q1 data assimilation to the WRF-CHEM model

The IGBP layer in MCD12Q1 is suitable for the WRF-CHEM IGBP land cover scheme, which consist of 11 natural vegetation classes, 3 developed and mosaicked land classes, and three non-vegetated land classes. Table S1 displays the comparison of land cover classification between the WRF-CHEM model and MCD12Q1. We use the gridded LCF of each category to assimilate the MCD12Q1 satellite data to the WRF-CHEM model.

$$LCF_{i,j,k} = \frac{Area_{i,j,k}}{Area_{i,j}} \quad (4)$$

Where i and j are grid cell indices of the WRF-CHEM model domain, $Area_{i,j,k}$ stands for the total area of each land cover category k within grid cell (i, j), and $Area_{i,j}$ is the area of grid cell (i, j). The $LCF_{i,j,k}$ ranges from 0 to 1.

To evaluate the afforestation impacts on the haze pollution in BTH, we have used and modified the coupled unified Noah land-surface model (LSM), which was developed based on Oregon State University LSM (Chen and Dudhia, 2001). The Noah is able to reasonably reproduce the observed diurnal variation of sensible heat fluxes and surface skin temperature. Also, it is capable of capturing the diurnal and seasonal evolution in evaporation and soil moisture (Chen et al., 1996). Despite some remaining issues, the Noah has been chosen for further refinement and implementation in NCEP regional and global coupled weather and climate models because of its relative simplicity and adequate performance (Mitchell, 2005).

The surface roughness length (SFz0) in Noah is calculated based on the dominant land cover category (https://ral.ucar.edu/solutions/products/unified-noah-lsm).

$$SFz0 = \begin{cases} SFz0_{min}, & G_T \le G_{min} \\ (1 - G_f) * SFz0_{min} + G_f * SFz0_{max}, & G_{min} \le G_T \le G_{max} \\ SFz0_{max}, & G_T \gg G_{max} \end{cases} \quad (5)$$

Where $SFz0_{min}$ and $SFz0_{max}$ are the minimal and maximum SFz0 for each category. G_f is the area fractional coverage of green vegetation, and G_T, G_{min} and G_{max} are the threshold, minimal, and maximal value of G_f, respectively. G_T, $SFz0_{min}$ and $SFz0_{max}$ are listed in Table S2.

In order to more precisely simulate surface stress within the sub-grid scale in heterogeneous terrain, the effective roughness length has been extensively studied, especially in the 1990s. Claussen (1990) has defined the effective roughness length as a value of the area average of the roughness length in heterogeneous terrain. The effective roughness length relies upon the blending height (Wieringa, 1986; Mason, 1988; Wood and Mason, 1991; Philip, 1996; Mahrt, 1996), at which the flow is approximately in equilibrium with underlying surface conditions and independent of horizontal position (Ma and Daggupary, 1998). We have modified the Noah SFz0 calculation using the spatial average of the vegetation roughness length.

$$SFz0 = \sum_k LCF_k * SFz0_k \quad (6)$$

$SFz0_k$ denotes the gridded area fraction of land cover category *k,* and calculated by Eq. (5).

3 Results and Discussions

3.1 Land cover change in BTH

The land cover in BTH and Beijing exhibits appreciable variation from 2001 to 2013 (Figure 2 and Table 2). In BTH, forests and croplands have increased by 7.2% and 1.9%, while shrublands and grasslands/savannas have decreased by 3.9% and 5.1%, respectively. In Beijing,

forests have increased by 14.9%, while shrublands have decreased by 12.6%. Apparently, the forest LCF has increased substantially in western and northern BTH, concentrated in the Taihang and Yanshan Mountains, with an increase up to 50%. This result is consistent with the previous study of Li et al. (2016), which has reported a remarkable forest growth in the northwest of NCP from 2000 to 2010. As such, a "Green Great Wall" has been established (Figure 2a), which has reportedly protected the southeastern BTH from the dust pollution (Liu et al., 2008; Duan et al., 2011; Parungo et al., 2013). The land cover change, particularly the evident forest growth, is primarily attributed to the China's national afforestation programs aiming to increase the forest coverage and to conserve soil and water, including the Grain for Green Project, the Three Norths Shelter Forests System Project (Phase IV), and the Natural Forest Conservation Program (Yin et al., 2010; Cao et al., 2011).

3.2 Model performance

We have first assimilated into the WRF-CHEM model the MCD12Q1 product of 2013 and performed the numerical simulation of haze pollution episodes from 1 December 2013 to 31 January 2014. For the discussion convenience, we have defined the simulation with the 2013 land cover as the reference case (hereafter referred to as REF case), and results from the reference simulation are compared to observations in BTH.

Considering the key role of meteorological fields in determining the formation, transformation, diffusion, transport, and removal of the air pollutants (Bei et al., 2017), Figure S2 presents the comparison of the simulated wind speed and direction, and planetary boundary layer height with the reanalysis data from ECMWF (European Centre for Medium-range Weather Forecasts) at monitoring sites. The predicted temporal variations of the three meteorological parameters are generally in agreement with the reanalysis data, with the *IOAs* exceeding 0.80, and the absolute *NMB* less than 25%.

Figure 3 presents the calculated and observed temporal profiles of near-surface air

207 pollutants concentrations averaged at monitoring sites in BTH during the simulation period,
208 including $PM_{2.5}$, O_3, NO_2, SO_2, and CO. The WRF-CHEM model generally reproduces the
209 haze pollution episodes well, e.g. all the haze events during the period are captured
210 successfully (Figure 3a), with an *IOA* of 0.90 and a *NMB* of 2.1% for $PM_{2.5}$ mass
211 concentrations. The model reasonably yields O_3 variations compared to observations, with an
212 *IOA* of 0.80, but underestimates O_3 concentrations, with a *NMB* of -15.9% (Figure 3b). In
213 winter, the insolation is weak in the north of China, unfavorable for the O_3 photochemical
214 production, so the O_3 level is substantially influenced by the boundary conditions. Hence, one
215 of possible reasons for the O_3 underestimation might be from the uncertainty in the O_3
216 boundary conditions. The simulated temporal variations of NO_2 mass concentrations are well
217 consistent with the observation, and the *IOA* and *NMB* are 0.91 and 0.6%, respectively. The
218 SO_2 and CO temporal variations are also reasonably replicated against observations, with
219 *IOAs* of 0.82 and 0.84, respectively.

220 Figure 4 shows the spatial comparison of calculated and observed $PM_{2.5}$ concentrations.
221 Generally, the average predicted $PM_{2.5}$ spatial patterns agree well with the observations at the
222 monitoring sites in BTH during the whole period (Figure 4b) and each month (Figures 4c and
223 4d), with *R*s exceeding 0.85, indicating good agreement of simulations with observations.
224 The observed $PM_{2.5}$ concentrations frequently exceed 150 μg m^{-3} in BTH, showing the
225 frequent occurrence of heavy haze pollution events. The model generally yields the observed
226 high $PM_{2.5}$ concentrations in BTH and their surrounding areas, although the model
227 underestimation or overestimation still exists. Additionally, compared to observations, the
228 model performs also well in simulating the spatial pattern of haze episodes with various
229 time-scales ranging from 8 to 16 days (Figure S3).

230 The good agreements of the simulated mass concentrations of air pollutants with
231 observations at monitoring sites in BTH show that the emission inventory used in present

study and simulated wind fields are generally reasonable, providing a reliable base for the further assessment. It is worth noting that, although the predicted meteorological parameters are generally consistent with the reanalysis data from ECMWF at monitoring sites, other factors still affect the meteorological field simulations and cause biases to compensate some of the deficiencies of the WRF-CHEM model, such as overestimation of surface wind speeds.

3.3 Effect of afforestation on haze pollution in BTH

Change in the land cover alters the surface roughness height (SFz0) that plays an important role in determining the surface level wind speed and energy exchange between the atmosphere and the land surface. Numerous studies have demonstrated that increasing SFz0 tends to decelerate the surface wind (Wu et al., 2016a, b), obstructing the dispersion of air pollutants (Sun et al., 2016; Zhao et al., 2013; Tie et al., 2015). In order to evaluate the impact of the afforestation induced SFz0 change and resultant dynamical change (e.g., wind field) on the haze formation, a sensitivity experiment is designed, in which the MCD12Q1 product of 2001 is assimilated into the WRF-CHEM model to represent the land cover situations before the afforestation (hereafter referred to as SEN-AFF case).

Figures 5a and 5b display the SFz0 change and its correlation with forest LCF change from 2001 to 2013, respectively. The land cover change considerably alters the SFz0, particularly in the afforestation area, with a SFz0 increase ranging from 0.1 to 0.3 m. Apparently, the SFz0 exhibits a distinct increasing trend in western and northern BTH, concentrated in the Taihang and Yanshan Mountains, which is well consistent with the increase of the forest LCF. The SFz0 change is highly correlated with the forest LCF change, with a correlation coefficient of 0.91. Generally, the SFz0 is mainly dependent upon the LCF (Equation 6), and sensitive to the forest change (Table S2). Therefore, afforestation constitutes the most important factor for the increase in the SFz0 in BTH.

It is worth noting that Jiménez and Dudhia (2012) have point out that there still exist

large uncertainties in parameterizing the air land interaction over complex terrain. Besides the vegetation effect on the roughness length, drag of subgrid features of topography need to be considered. The parameterization of orographic flow over complex terrain is a challengeable problem at the mesoscale numerical simulation. In early versions of the WRF model, a large bias in predicting surface winds over complex terrain has occurred due to the drag exerted by unresolved topography (Cheng and Steenburgh, 2005). Great efforts have been made to improve the simulation of orographic flow over complex terrain. The new parameterization scheme introduced in the WRF model since version 3.4.1 has corrected this high wind speed bias over plains and valleys (Mughal et al., 2017), and also corrected the low wind speed bias found over the mountains and hills (Jiménez and Dudhia, 2012).

Figures 5c and 5d illustrate the influence of the afforestation on the surface $PM_{2.5}$ and wind field averaged during the simulation period (defined as (REF − SEN-AFF)). The prevailing westerly or northerly wind is decelerated in the western and northwestern BTH due to the increased SFz0 caused by the afforestation, with the wind speed decrease ranging from 0.3~1.5 m s^{-1}. The afforestation tends to deteriorate the haze pollution in BTH, particularly in the downwind area of the afforestation, with the period average $PM_{2.5}$ enhancement reaching about 6~15 μg m^{-3}, or 3~6%. The $PM_{2.5}$ enhancement in Beijing is the most evident, corresponding to the rapid growth of forests in the west and in/on the north of Beijing. Furthermore, during each episode, the afforestation generally tends to deteriorate the haze pollution in BTH, enhancing the $PM_{2.5}$ concentration by about up to 3~6%, particularly in the downwind area of the afforestation (Figure S4). On average, the difference of the simulated air pollutants and meteorological parameters between the REF and SEN-AFF case is not significant (Figures 5c and 5d).

The occurrence of heavy haze pollution in BTH is generally associated with the weakening of northerly or northwesterly winds, which facilitates the accumulation of air

282 pollutants in BTH. The afforestation in the western and northwestern BTH increases SFz0,
283 further decelerating northerly or northwesterly winds and deteriorating the haze pollution.
284 However, the afforestation only plays a marginal role in worsening the haze pollution, and
285 does not constitute the main cause for the heavy haze formation.

286 Apparently, during the haze development, when the northerly or northwesterly wind is
287 weak or becomes calm, the SFz0 increase due to the afforestation contributes negligibly to
288 the haze deterioration in BTH. However, once the northerly or northwesterly wind
289 commences to strengthen but is not strong enough to evacuate the air pollutants in BTH, the
290 SFz0 increase would play an appreciable role in sustaining high $PM_{2.5}$ levels in the
291 downwind area of the afforestation. Figure 6 presents the $PM_{2.5}$ contribution of the
292 afforestation during the occurrence of a northerly gust on January 18, 2014. The intensified
293 northerly wind cleanses the northern BTH, but the haze pollution is still very severe in the
294 southern BTH. The afforestation considerably elevates the $PM_{2.5}$ concentration in
295 southeastern BTH, particularly in Beijing and Tianjin, with the $PM_{2.5}$ contribution exceeding
296 up to 15% (Figure 6b).

297 It is worth noting that the aerosol species (organic aerosol, sulfate, nitrate, ammonium,
298 and elemental carbon) exhibit the same variation trend as the $PM_{2.5}$ due to the afforestation
299 (Figure S5). Apparently, the organic aerosol is the major contributor to the $PM_{2.5}$ variation
300 due to the afforestation, followed by the sulfate and ammonium aerosol. The afforestation
301 also increases emissions of the biogenic SOA (BSOA) precursors, such as isoprene and
302 monoterpenes. However, due to the very low emissions of BSOA precursors during
303 wintertime (Guenther et al., 2006; 2012), the BSOA contribution to $PM_{2.5}$ concentrations is
304 insignificant, less than 3 $\mu g\ m^{-3}$ on average during the whole episodes (Figure S6a). The
305 average BSOA enhancement due to the afforestation is less than 0.5% (Figure S6b).
306 Furthermore, in general, the afforestation has little effect on the boundary layer height,

upward sensible heat flux (associated with turbulent mixing), and moisture (related to clouds) in BTH (Figure S7).

To assess the upper limit of impacts of the afforestation on the $PM_{2.5}$ level in BTH, two additional experiments are conducted and compared to the REF case. The two experiments are one with complete deforestation and the other with complete afforestation in the Taihang and Yanshan Mountains (Figures 7a and 7c). In the complete deforestation sensitivity case, the barren surface with SFz0 of 0.01 m is used to replace other land cover categories. In the complete afforestation case, the deciduous broadleaf forest category with SFz0 of 0.5 m is used to replace other land cover categories. As shown in Figure 7, complete deforestation considerably decreases the $PM_{2.5}$ level in BTH, with the period average $PM_{2.5}$ reduction ranging from 5~18 μg m^{-3} generally, and in particular, the $PM_{2.5}$ concentration in Beijing is reduced by more than 10 μg m^{-3}, due to the intensified northerly or northwesterly wind caused by the decrease of SFz0 in the Taihang and Yanshan Mountains. Complete afforestation deteriorates the haze pollution in BTH, and the haze pollution maintains in the Taihang and Yanshan Mountains due to the weakened northerly or northwesterly wind. Additionally, the enhancement of $PM_{2.5}$ concentrations in foothill of Taihang and Yanshan Mountains is obvious, varying from 10 to 25 μg m^{-3} (Figure 7d).

Interestingly, the afforestation deteriorates most to the haze pollution in Beijing (see Figure 5). So it is anticipated that the proposed large ventilation corridor system could alleviate the haze pollution in Beijing (China forest network, 2014, 2016b, c). Originally, the ventilation corridor system was devised to relieve the urban heat island effect and improve the thermal environmental conditions in the urbanized regions. With the frequent occurrence of heavy haze in Beijing, the debatable system is expected to blow away the haze and bring blue sky to Beijing. In order to examine the effects of the wind corridor system, a sensitivity experiment is conducted based on the base case, in which three artificial ventilation corridors

are designed in the northwest, north, and northeast of Beijing, with a width of 6 km (Figure 8a). For all the grid cells within the corridors, the barren surface with SFz0 of 0.01 m is used to replace other land cover categories. Contrast to the anticipation, our sensitivity results show that the $PM_{2.5}$ reduction due to the designed ventilation corridor system is less than 1% in Beijing (Figure 8b). Note that the width of the ventilation corridor in the sensitivity study is 12 times of the proposed one. Hence, the proposed large ventilation corridor system is not effective or beneficial to mitigate the haze pollution in Beijing.

4 Summary and conclusions

The annual land cover product, MCD12Q1, derived from the MODIS observations since 2001 has been used to analyze the land cover change in BTH. A considerable increasing trend of forests in the western and northwestern BTH has been identified, which is caused by the China's national afforestation programs. Forests in BTH and Beijing have increased by 7.2% and 14.9%, respectively, from 2001 to 2013. The fast forest expansion has increased the surface roughness height, particularly in Beijing and its surrounding areas.

The MCD12Q1 product of 2013 has been assimilated into the WRF-CHEM model to represent the current land cover condition. Persistent haze pollution episodes in BTH from 1 December 2013 to January 2014 are simulated using the WRF-CHEM model. Generally, the WRF-CHEM model reasonably well reproduces the temporal variations and spatial distributions of air pollutants compared to observations at monitoring sites in BTH.

Sensitivity studies have demonstrated that the increase of the surface roughness height decreases the northwesterly or northerly wind speed in the western and northwestern BTH by about 0.3~1.5 m s^{-1}. The haze pollution is deteriorated in BTH to some degree, and $PM_{2.5}$ concentrations are generally enhanced by less than 6% due to the afforestation. The heavy haze formation in BTH is generally associated with meteorological conditions when the

northerly or northwesterly wind is weak. Once the northerly or northwesterly wind is strengthened during the haze development in BTH, afforestation plays a considerable role in maintaining high $PM_{2.5}$ concentrations in the downwind of the afforestation area. Complete afforestation or deforestation in the Taihang and Yanshan Mountains would increase or decrease the $PM_{2.5}$ level within 15% in BTH.

Additionally, our model results do not support that the proposed large ventilation corridor system is beneficial to alleviate the haze pollution in Beijing. Under the unfavorable synoptic situations, emissions mitigation is the solely optimum approach to mitigate the haze pollution in BTH.

It is worth to note that, in the present study, contributions of the surface roughness change induced by afforestation to the haze pollution are primarily evaluated using the WRF-CHEM model, but many other factors which directly or indirectly influence air quality, are also modified by the land cover change, including surface moisture, terrestrial erosion, pollutants' dry deposition, PBL thermal stability, etc. For example, changes in surface moisture and surface erosion impact the emissions of natural particles; changes in dry deposition directly influence the air quality in situ and indirectly the air quality downwind with occurrence of recirculation. Therefore, when changes in all those factors caused by land cover change are accounted for, the role of afforestation in air quality in situ might be uncertain. In the online WRF-CHEM model, besides the surface roughness, the impacts of afforestation on the heat flux, surface moisture, surface erosion, and dry deposition of air pollutants have also been considered. Considering that afforestation in BTH is mainly distributed in the mountain region, the surface roughness increase induced by afforestation obviously decrease surface wind speeds, facilitating accumulation of air pollutants in the downwind region and further deteriorating the haze pollution.

5 Data availability

The real-time $PM_{2.5}$, O_3, NO_2, SO_2, and CO mass concentrations are accessible to the public on the website http://106.37.208.233:20035/. One can also access the historic profiles of the observed ambient air pollutants by visiting http://www.aqistudy.cn/.

Acknowledgements. This work was financially supported by National Key R&D Plan (Quantitative Relationship and Regulation Principle between Regional Oxidation Capacity of Atmospheric and Air Quality (2017YFC0210000)). Long Xin was supported by the Fundamental Research Funds for the Central Universities, and the Project funded by China Postdoctoral Science Foundation (no. 2016M602886) and the Shaanxi Postdoctoral Science Foundation (no. 2017BSHYDZZ27). Guohui Li is supported by "Hundred Talents Program" of the Chinese Academy of Sciences and the National Natural Science Foundation of China (No. 41661144020).

400 **Reference**

401 Bai, Y., Feng, M., Jiang, H., Wang, J., and Liu, Y.: Validation of land cover maps in China
402 using a sampling-based labeling approach, Remote SENS-BASEL, 7, 10589-10606,
403 2015.

404 Bei, N., Li, G., and Molina, L. T.: Uncertainties in SOA simulations due to meteorological
405 uncertainties in Mexico City during MILAGRO-2006 field campaign, Atmos. Chem.
406 Phys., 12, 16293-16326, 2012.

407 Bei, N., Wu, J., Elser, M., Feng, T., Cao, J., El-Haddad, I., Li, X., Huang, R., Li, Z., Long, X.,
408 Xing, L., Zhao, S., Tie, X., Prévôt, A. S. H., and Li, G., 2017. Impacts of meteorological
409 uncertainties on the haze formation in Beijing-Tianjin-Hebei (BTH) during wintertime: a
410 case study. Atmos. Chem. Phys., 17, 14579-14591, doi: 10.5194/acp-17-14579-2017.

411 Bichet, A., Wild, M., Folini, D., and Schar, C.: Causes for decadal variations of wind speed
412 over land: Sensitivity studies with a global climate model, Geophy. Res. Lett., 39, 2012.

413 Binkowski, F. S., and Roselle, S. J.: Models-3 Community Multiscale Air Quality (CMAQ)
414 model aerosol component 1. Model description, J. Geophys. Res., 108, 2003.

415 Cao, S., Chen, L., Shankman, D., Wang, C., Wang, X., and Zhang, H.: Excessive reliance on
416 afforestation in China's arid and semi-arid regions: lessons in ecological restoration,
417 Earth-Sci. Rev., 104, 240-245, 2011.

418 Chen, F., Mitchell, K., Schaake, J., Xue, Y., Pan, H. L., Koren, V., Duan, Q. Y., Ek, M., and
419 Betts, A.: Modeling of land surface evaporation by four schemes and comparison with
420 FIFE observations, J. Geophys. Res. Atmos., 101, 7251-7268, 1996.

421 Chen, F., and Dudhia, J.: Coupling an advanced land surface–hydrology model with the Penn
422 State–NCAR MM5 modeling system. Part II: Preliminary model validation, Mon.
423 Weather Rev., 129, 587-604, 2001.

424 Chen, L., Li, D., and Pryor, S. C.: Wind speed trends over China: quantifying the magnitude
425 and assessing causality, Int. J. Climatol., 33, 2579-2590, 2013.

426 Cheng, W. Y. Y., and Steenburgh, W. J.: Evaluation of surface sensible weather forecasts by
427 the WRF and the Eta Models over the western United States, Weather Forecast., 20,
428 812-821, 10.1175/waf885.1, 2005.

429 China forestry network, http://www.forestry.gov.cn/portal/main/s/2103/content-686660.html,
430 access: 27 November, 2014.

431 China forestry network, http://www.forestry.gov.cn/thw/1807/content-834072.html, access:
432 27 November, 2016a.

433 China forestry network, http://www.forestry.gov.cn/main/2103/content-857797.html, access:
434 27 November, 2016b.

435 China forestry network, http://www.forestry.gov.cn/main/2103/content-872159.html, access:
436 27 November, 2016c.

437 China forestry network, http://www.forestry.gov.cn/zlszz/4253/content-936157.html, access:
438 27 November, 2017.

439 Claussen, M.: Area-averaging of surface fluxes in a neutrally stratified, horizontally
440 inhomogeneous atmospheric boundary layer, Atmos. Environ., 24, 1349-1360, 1990.

441 Chou, M.-D., and Suarez, M. J.: A solar radiation parameterization for atmospheric studies,
442 NASA Tech. Memo, 15, 40, 1999.

443 Chou, M.-D., Suarez, M. J., Liang, X.-Z., Yan, M. M.-H., and Cote, C.: A thermal infrared
444 radiation parameterization for atmospheric studies, Tech. Rep. NASA/TM-2001-104606,
445 19, 55, 2001.

446 Duan, H., Yan, C., Tsunekawa, A., Song, X., Li, S., and Xie, J.: Assessing vegetation
447 dynamics in the Three-North Shelter Forest region of China using AVHRR NDVI data,
448 Environ. Earth Sci., 64, 1011-1020, 2011.

449 Emmons, L. K., Walters, S., Hess, P. G., Lamarque, J. F., Pfister, G. G., Fillmore, D., Granier,
450 C., Guenther, A., Kinnison, D., and Laepple, T.: Description and evaluation of the
451 Model for Ozone and Related chemical Tracers, version 4 (MOZART-4), Geosci.
452 Model Dev., 3, 43-67, 2010.

453 Friedl, M. A., McIver, D. K., Hodges, J. C., Zhang, X., Muchoney, D., Strahler, A. H.,
454 Woodcock, C. E., Gopal, S., Schneider, A., and Cooper, A.: Global land cover mapping
455 from MODIS: algorithms and early results, Remote Sens. Environ., 83, 287-302, 2002.

456 Friedl, M. A., Sulla-Menashe, D., Tan, B., Schneider, A., Ramankutty, N., Sibley, A., and
457 Huang, X.: MODIS Collection 5 global land cover: Algorithm refinements and
458 characterization of new datasets, Remote Sens. Environ., 114, 168-182, 2010.

459 Gerten, D., Schaphoff, S., Haberlandt, U., Lucht, W., and Sitch, S.: Terrestrial vegetation and
460 water balance—hydrological evaluation of a dynamic global vegetation model, J.
461 Hydrol., 286, 249-270, 2004.

462 Grell, G. A., Peckham, S. E., Schmitz, R., McKeen, S. A., Frost, G., Skamarock, W. C., and
463 Eder, B.: Fully coupled "online" chemistry within the WRF model, Atmos. Environ., 39,
464 6957-6975, 2005.

465 Guenther, C.: Estimates of global terrestrial isoprene emissions using MEGAN (Model of
466 Emissions of Gases and Aerosols from Nature), Atmos. Chem. Phys., 6, 2006.

467 Guenther, A. B., Jiang, X., Heald, C. L., Sakulyanontvittaya, T., Duhl, T., Emmons, L. K.,
468 and Wang, X.: The Model of Emissions of Gases and Aerosols from Nature version 2.1
469 (MEGAN2.1): an extended and updated framework for modeling biogenic emissions,
470 Geosci. Model Dev., 5, 1471-1492, https://doi.org/10.5194/gmd-5-1471-2012, 2012.

471 Hong, S.-Y., and Lim, J.-O. J.: The WRF Single-Moment 6-Class Microphysics Scheme
472 (WSM6), Asia-Pac. J. Atmos. Sci., 42, 129-151, 2006.

473 Horowitz, L. W., Walters, S., Mauzerall, D. L., Emmons, L. K., Rasch, P. J., Granier, C., Tie,
474 X. X., Lamarque, J. F., Schultz, M. G., Tyndall, G. S., Orlando, J. J., and Brasseur, G. P.:
475 A global simulation of tropospheric ozone and related tracers: Description and
476 evaluation of MOZART, version 2, J. Geophys. Res. Atmos., 108, 4784,
477 doi:10.1029/2002jd002853, 2003.

478 Huang, T., Zhang, X., Ling, Z., Zhang, L., Gao, H., Tian, C., Guo, J., Zhao, Y., Wang, L., and

Ma, J.: Impacts of Large-Scale Land-Use Change on the Uptake of Polycyclic Aromatic Hydrocarbons in the Artificial Three Northern Regions Shelter Forest Across Northern China, Environ. Sci. Technol., 50, 12885, 2016.

Jiménez, P. A., and Dudhia, J.: Improving the representation of resolved and unresolved topographic effects on surface wind in the WRF Model, J. Appl. Meteorol. Clim., 51, 300-316, 2012.

Janjić, Z. I.: Nonsingular implementation of the Mellor–Yamada level 2.5 scheme in the NCEP Meso model, NCEP office note, 437, 61, 2002.

Li, G., Zhang, R., Fan, J., and Tie, X.: Impacts of black carbon aerosol on photolysis and ozone, J. Geophys. Res., 110, 2005.

Li, G., Lei, W., Zavala, M., Volkamer, R., Dusanter, S., Stevens, P., and Molina, L.: Impacts of HONO sources on the photochemistry in Mexico City during the MCMA-2006/MILAGO Campaign, Atmos. Chem. Phys., 10, 6551-6567, 2010.

Li, G., Bei, N., Tie, X., and Molina, L.: Aerosol effects on the photochemistry in Mexico City during MCMA-2006/MILAGRO campaign, Atmos. Chem. Phys., 11, 5169-5182, 2011a.

Li, G., Zavala, M., Lei, W., Tsimpidi, A., Karydis, V., Pandis, S. N., Canagaratna, M., and Molina, L.: Simulations of organic aerosol concentrations in Mexico City using the WRF-CHEM model during the MCMA-2006/MILAGRO campaign, Atmos. Chem. Phys., 11, 3789-3809, 2011b.

Li, G., Lei, W., Bei, N., and Molina, L.: Contribution of garbage burning to chloride and PM 2.5 in Mexico City, Atmos. Chem. Phys., 12, 8751-8761, 2012.

Li, G., Bei, N., Cao, J., Wu, J., Long, X., Feng, T., Dai, W., Liu, S., Zhang, Q., and Tie, X.: Widespread and persistent ozone pollution in eastern China during the non-winter season of 2015: observations and source attributions, Atmos. Chem. Phys., 17, 1-39, 2017.

Li, X., Wang, H., Zhou, S., Sun, B., and Gao, Z.: Did ecological engineering projects have a significant effect on large-scale vegetation restoration in Beijing-Tianjin Sand Source Region, China? A remote sensing approach, Chinese Geogr. Sci., 26, 216-228, 2016.

Lim, S. S., Vos, T., Flaxman, A. D., Danaei, G., Shibuya, K., Adair-Rohani, H., AlMazroa, M. A., Amann, M., Anderson, H. R., and Andrews, K. G.: A comparative risk assessment of burden of disease and injury attributable to 67 risk factors and risk factor clusters in 21 regions, 1990–2010: a systematic analysis for the Global Burden of Disease Study 2010, The lancet, 380, 2224-2260, 2013.

Liu, J. G., Li, S. X., Ouyang, Z. Y., Tam, C., and Chen, X. D.: Ecological and socioeconomic effects of China's policies for ecosystem services, Proc. Natl. Acad. Sci. U. S. A., 105, 9477-9482, 2008.

Ma, J., and Daggupaty S. M.: Stability Dependence of Height Scales and Effective Roughness Lengths of Momentum and Heat Transfer Over Roughness Changes, Bound. Lay. Meteorol., 88, 145-160, 1998.

519 Mahrt, L.: The bulk aerodynamic formulation over heterogeneous surfaces, Bound.-Lay.
520 Meteorol., 78, 87-119, 1996.

521 Mason, P. J.: The formation of area-averaged roughness lengths. Quart. J. Roy. Meteorol.
522 Soc., 114, 399-420, 1988.

523 McVicar, T. R., Roderick, M. L., Donohue, R. J., Li, L. T., Van Niel, T. G., Thomas, A.,
524 Grieser, J., Jhajharia, D., Himri, Y., Mahowald, N. M., Mescherskaya, A. V., Kruger, A.
525 C., Rehman, S., and Dinpashoh, Y.: Global review and synthesis of trends in observed
526 terrestrial near-surface wind speeds: Implications for evaporation, J. Hydrol., 416,
527 182-205, 2012.

528 Mitchell, K.: The Community Noah Land-Surface Model (LSM). User's Guide. Public
529 Release Version 2.7.1, 2017, 2005.

530 Mughal, M. O., Lynch, M., Yu, F., Mcgann, B., Sutton, J., and Sutton, J.: Wind modelling,
531 validation and sensitivity study using Weather Research and Forecasting model in
532 complex terrain, Environ. Modell. Softw., 90, 107-125, 2017.

533 Nenes, A., Pandis, S. N., and Pilinis, C.: ISORROPIA: A new thermodynamic equilibrium
534 model for multiphase multicomponent inorganic aerosols, Aquat. geochem., 4, 123-152,
535 1998.

536 Parungo, F., Li, Z., Li, X., Yang, D., and Harris, J.: Gobi dust storms and The Great Green
537 Wall, Geophy. Res. Lett., 21, 999-1002, 2013.

538 Reichstein, M., Ciais, P., Papale, D., Valentini, R., Running, S., Viovy, N., Cramer, W.,
539 Granier, A., Ogee, J., and Allard, V.: Reduction of ecosystem productivity and
540 respiration during the European summer 2003 climate anomaly: a joint flux tower,
541 remote sensing and modelling analysis, Global Change Biol., 13, 634-651, 2007.

542 Philip, J. R.: Two-dimensional checkerboards and blending heights, Bound. Lay. Meteorol.,
543 80, 1-18, 1996.

544 Sun, Y., Chen, C., Zhang, Y., Xu, W., Zhou, L., Cheng, X., Zheng, H., Ji, D., Li, J., and Tang,
545 X.: Rapid formation and evolution of an extreme haze episode in Northern China during
546 winter 2015, Sci. Rep., 6, 27151, 2016.

547 Tie, X., Zhang, Q., He, H., Cao, J., Han, S., Gao, Y., Li, X., and Jia, X. C.: A budget analysis
548 of the formation of haze in Beijing, Atmos. Environ., 100, 25-36, 2015.

549 Streets, D. G., Zhang, Q., Wang, L., He, K., Hao, J., Wu, Y., Tang, Y., and Carmichael, G. R.:
550 Revisiting China's CO emissions after the Transport and Chemical Evolution over the
551 Pacific (TRACE-P) mission: Synthesis of inventories, atmospheric modeling, and
552 observations, J. Geophys. Res. Atmos., 111(D14), 2006.

553 Turner, B. L., Lambin, E. F., and Reenberg, A.: The emergence of land change science for
554 global environmental change and sustainability, Proc. Natl. Acad. Sci. U. S. A., 104,
555 20666-20671, 2007.

556 Vautard, R., Cattiaux, J., Yiou, P., Thépaut, J.-N., and Ciais, P.: Northern Hemisphere
557 atmospheric stilling partly attributed to an increase in surface roughness, Nat. Geosci., 3,
558 756-761, 2010.

559 Wang, S., and Hao, J.: Air quality management in China: Issues, challenges, and options, J.
560 Environ. Sci., 24, 2-13, 2012.

561 Wiedinmyer, C., Akagi, S. K., Yokelson, R. J., and Emmons, L. K.: The Fire INventory from
562 NCAR (FINN) – a high resolution global model to estimate the emissions from open
563 burning, Geosci. Model Dev. Discuss., 3, 625-641, 2011.

564 Wieringa, J.: Roughness-dependent geographical interpolation of surface wind speed
565 averages, Quart. J. Roy. Meteorol. Soc., 112, 867-889, 1986.

566 Wesely, M.: Parameterization of surface resistances to gaseous dry deposition in
567 regional-scale numerical models, Atmos. Environ., 23, 1293-1304, 1989.

568 Wood, N., and Mason, P.: The influence of static stability on the effective roughness lengths
569 for momentum and heat transfer, Quart. J. Roy. Meteorol. Soc., 117, 1025-1056, 1991.

570 Wu, J., Zha, J., and Zhao, D.: Evaluating the effects of land use and cover change on the
571 decrease of surface wind speed over China in recent 30 years using a statistical
572 downscaling method, Clim. Dynam., 1-19, 2016a.

573 Wu, J., Zha, J., and Zhao, D.: Estimating the impact of the changes in land use and cover on
574 the surface wind speed over the East China Plain during the period 1980–2011, Clim.
575 Dynam., 46, 847-863, 2016b.

576 Wu, J., Li, G., Cao, J., Bei, N., Wang, Y., Feng, T., Huang, R., Liu, S., Zhang, Q., and Tie, X.:
577 Contributions of trans-boundary transport to summertime air quality in Beijing, China,
578 Atmos. Chem. Phys., 17, 1-46, 2017.

579 Wu, W., Shibasaki, R., Ongaro, L., Ongaro, L., Zhou, Q., and Tang, H.: Validation and
580 comparison of 1 km global land cover products in China, Int. J. Remote Sens., 29,
581 3769-3785, 2008.

582 Yang, Y., Xiao, P., Feng, X., and Li, H.: Accuracy assessment of seven global land cover
583 datasets over China, Isprs J. Photogramm., 125, 156-173, 2017.

584 Yin, R. S., Yin, G. P., and Yin, R.: China's primary programs of terrestrial ecosystem
585 restoration: initiation, implementation, and challenges, Environ. Manage., 45, 429-441,
586 2010.

587 Zhang, Q., Streets, D. G., Carmichael, G. R., He, K. B., Huo, H., Kannari, A., Klimont, Z.,
588 Park, I. S., Reddy, S., Fu, J. S., Chen, D., Duan, L., Lei, Y., Wang, L. T., and Yao, Z. L.:
589 Asian emis- sions in 2006 for the NASA INTEX-B mission, Atmos. Chem. Phys., 9,
590 5131–5153, doi:10.5194/acp-9-5131-2009, 2009.

591 Zhao, X., Zhao, P., Xu, J., Meng, W., Pu, W., Dong, F., He, D., and Shi, Q.: Analysis of a
592 winter regional haze event and its formation mechanism in the North China Plain,
593 Atmos. Chem. Phy., 13, 5685-5696, 2013.

594 Zhang, X., Huang, T., Zhang, L., Gao, H., Shen, Y., and Ma, J.: Trends of deposition fluxes
595 and loadings of sulfur dioxide and nitrogen oxides in the artificial Three Northern
596 Regions Shelter Forest across northern China, Environ. Pollut., 207, 238-247, 2015.

597 Zhang, X., Du, J., Huang, T., Zhang, L., Gao, H., Zhao, Y., and Ma, J.: Atmospheric removal

of PM2.5 by man-made Three Northern Regions Shelter Forest in Northern China estimated using satellite retrieved PM2.5 concentration, Sci. Total Environ., 593-594, 713, 2017.

607 Table 1 WRF-CHEM model configurations

608

Simulation Regions	**Beijing-Tianjin-Hebei-Shandong**
Simulation period	1 December 2013 to 31 January 2014
Domain size	200 × 200
Domain center	38°N, 116°E
Horizontal resolution	6km × 6km
Vertical resolution	35 vertical levels with a stretched vertical grid with spacing ranging from 30 m near the surface, to 500 m at 2.5 km and 1 km above 14 km
Microphysics scheme	WSM 6-class graupel scheme (Hong and Lim, 2006)
Boundary layer scheme	MYJ TKE scheme (Janjić, 2002)
Surface layer scheme	MYJ surface scheme (Janjić, 2002)
Land-surface scheme	Unified Noah land-surface model (Chen and Dudhia, 2001)
Longwave radiation scheme	Goddard longwave scheme (Chou and Suarez, 2001)
Shortwave radiation scheme	Goddard shortwave scheme (Chou and Suarez, 1999)
Meteorological boundary and initial conditions	NCEP 1°×1° reanalysis data
Chemical initial and boundary conditions	MOZART 6-hour output (Horowitz et al., 2003)
Anthropogenic emission inventory	SAPRC-99 chemical mechanism emissions (Zhang et al., 2009)
Biogenic emission inventory	MEGAN model developed by Guenther et al. (2006)
Model spin-up time	28 hours

609
610
611
612
613

614 Table 2 Land cover change over Beijing and BTH from 2001 to 2013
615

Land cover categories	Land cover description	Beijing	BTH
1~5	Forests	14.9%	7.2%
6~7	Shrublands	-12.6%	-3.9%
12/14	Croplands	-0.1 %	1.9%
8~10	Grasslands	-2.0%	-5.1%
Others	~	-0.2%	-0.1%

616
617
618
619
620

Figure Captions

Figure 1 (a) The model domain, region of interest (ROI) and monitoring sites. (b) The topography and monitoring sites in January 2014. The circles represent the centers of cities with ambient monitoring sites and the size of circles denotes the number of monitoring sites in the cities. The boundary of BTH region is highlighted with bright lines. The Yanshan and Taihang Mountains are also displayed.

Figure 2 Land cover change from 2001 to 2013. Spatial distributions of (a) forests, (b) shrublands, (c) croplands, and (d) grasslands.

Figure 3 Comparisons of observed (black dots) and simulated (solid red lines) diurnal profiles of near-surface hourly mass concentrations of (a) $PM_{2.5}$, (b) O_3, (c) NO_2, (d) SO_2, and (d) CO averaged at monitoring sites in BTH from 1 December 2013 to 31 January 2014.

Figure 4 Pattern comparisons of calculated and observed near-surface $PM_{2.5}$ mass concentrations. (a) Spatial correlation between calculated and observed $PM_{2.5}$ concentrations during each month and the whole simulation period. Horizontal distribution of calculated (color contour) and observed (colored circles) average $PM_{2.5}$ concentrations during (b) the whole simulation period, (c) December 2013, and (d) January 2014, along with the simulated wind fields (black arrows).

Figure 5 (a) SFz0 change from 2001 to 2013, and (b) its correlation with the forest LCF change; Horizontal distribution of (c) absolute and (d) relative near-surface $PM_{2.5}$ mass concentration changes caused by the afforestation. The wind field changes are shown in black arrows in (c) and (d).

Figure 6 Horizontal distribution of (a) the average near surface $PM_{2.5}$ mass concentration and (b) its change due to the afforestation during an intensified northerly/northwesterly event from 00:00 to 10:00 Beijing Time on January 18, 2014. The wind field and its change are shown in black arrows.

Figure 7 Horizontal distribution of (a) the average near surface $PM_{2.5}$ mass concentration and (b) its change due to the afforestation during an intensified northerly/northwesterly event from 00:00 to 10:00 Beijing Time on January 18, 2014. The wind field and its change are shown in black arrows.

Figure 8 Impacts of an artificial large ventilation corridor system on (a) SFz0 and (b) average near-surface $PM_{2.5}$ mass concentrations from 1 December 2013 to 31 January 2014, along with the wind field (black arrows).

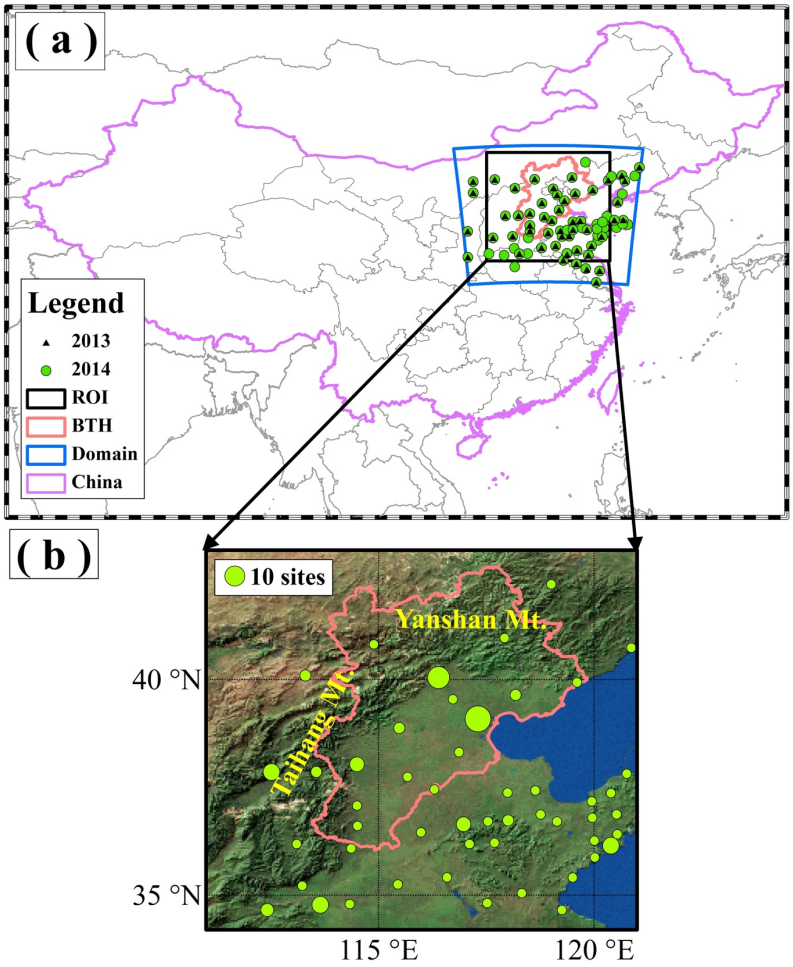

Figure 1 (a) The model domain, region of interest (ROI) and monitoring sites. (b) The topography and monitoring sites in January 2014. The circles represent the centers of cities with ambient monitoring sites and the size of circles denotes the number of monitoring sites in the cities. The boundary of BTH region is highlighted with bright lines. The Yanshan and Taihang Mountains are also displayed.

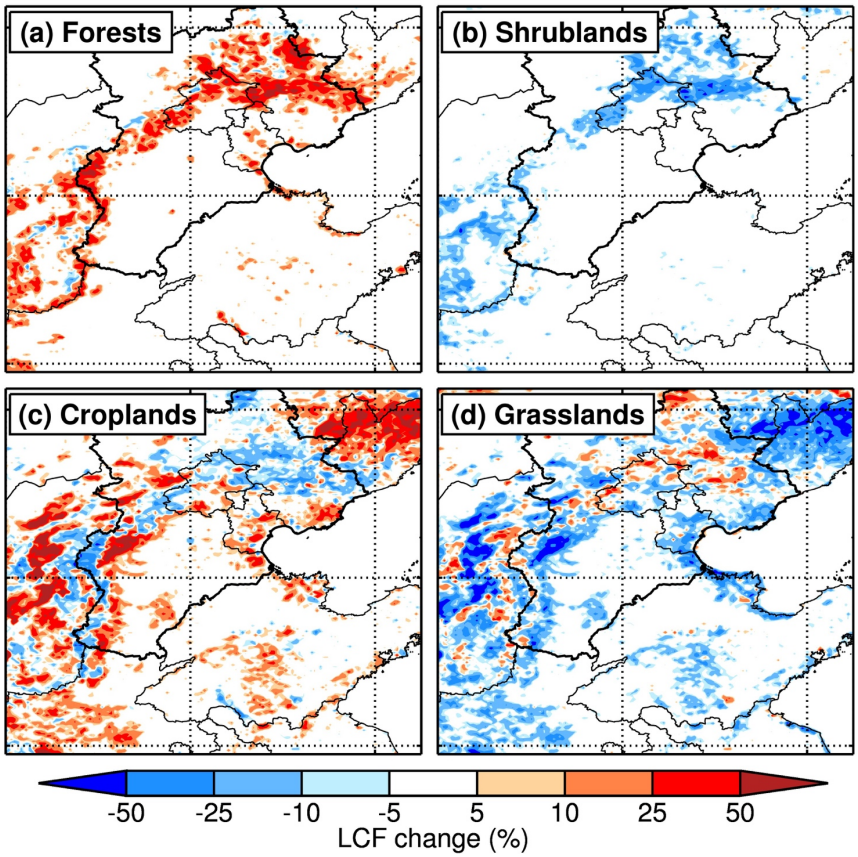

Figure 2 Land cover change from 2001 to 2013. Spatial distributions of (a) forests, (b) shrublands, (c) croplands, and (d) grasslands.

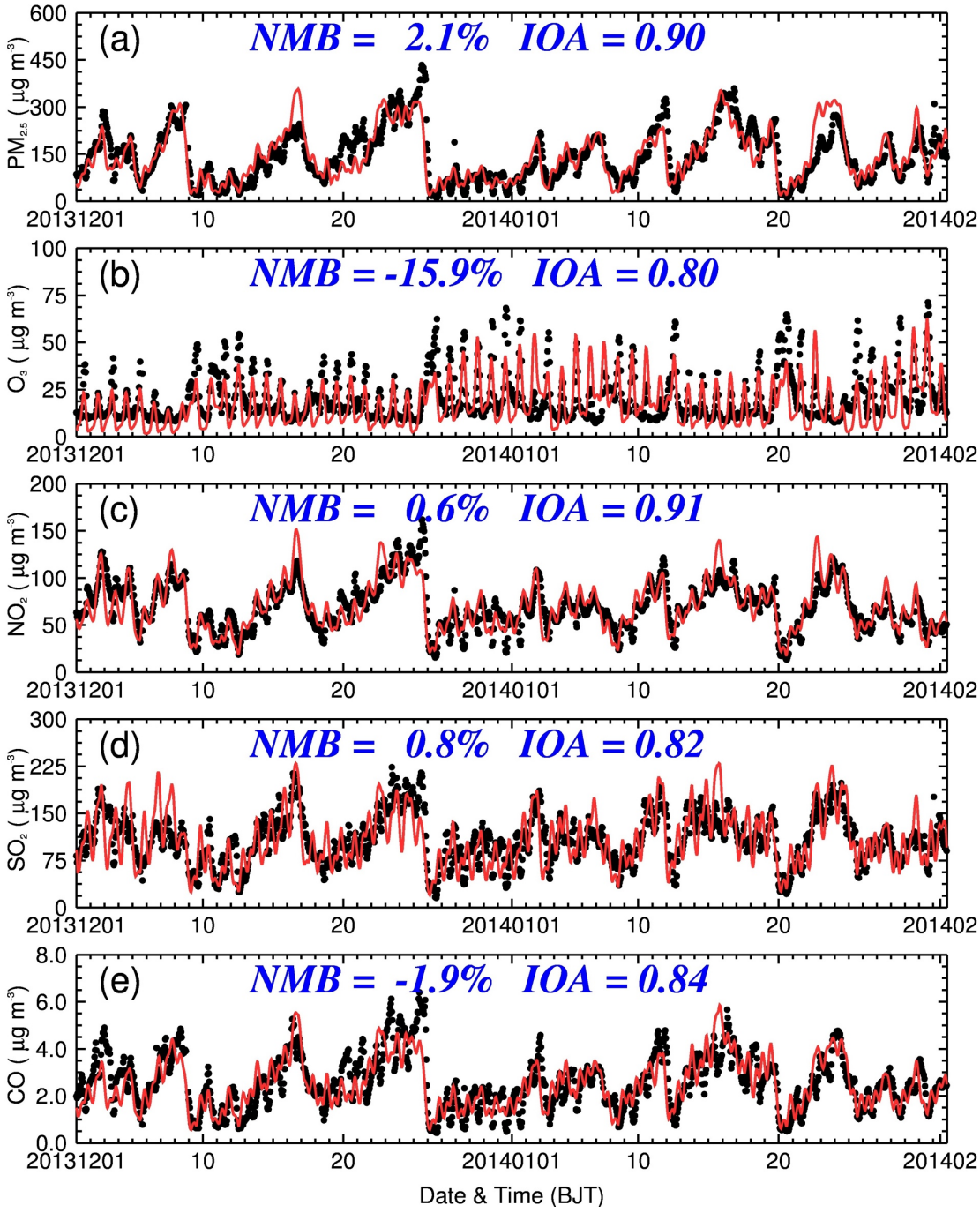

Figure 3 Comparisons of observed (black dots) and simulated (solid red lines) diurnal profiles of near-surface hourly mass concentrations of (a) $PM_{2.5}$, (b) O_3, (c) NO_2, (d) SO_2, and (d) CO averaged at monitoring sites in BTH from 1 December 2013 to 31 January 2014.

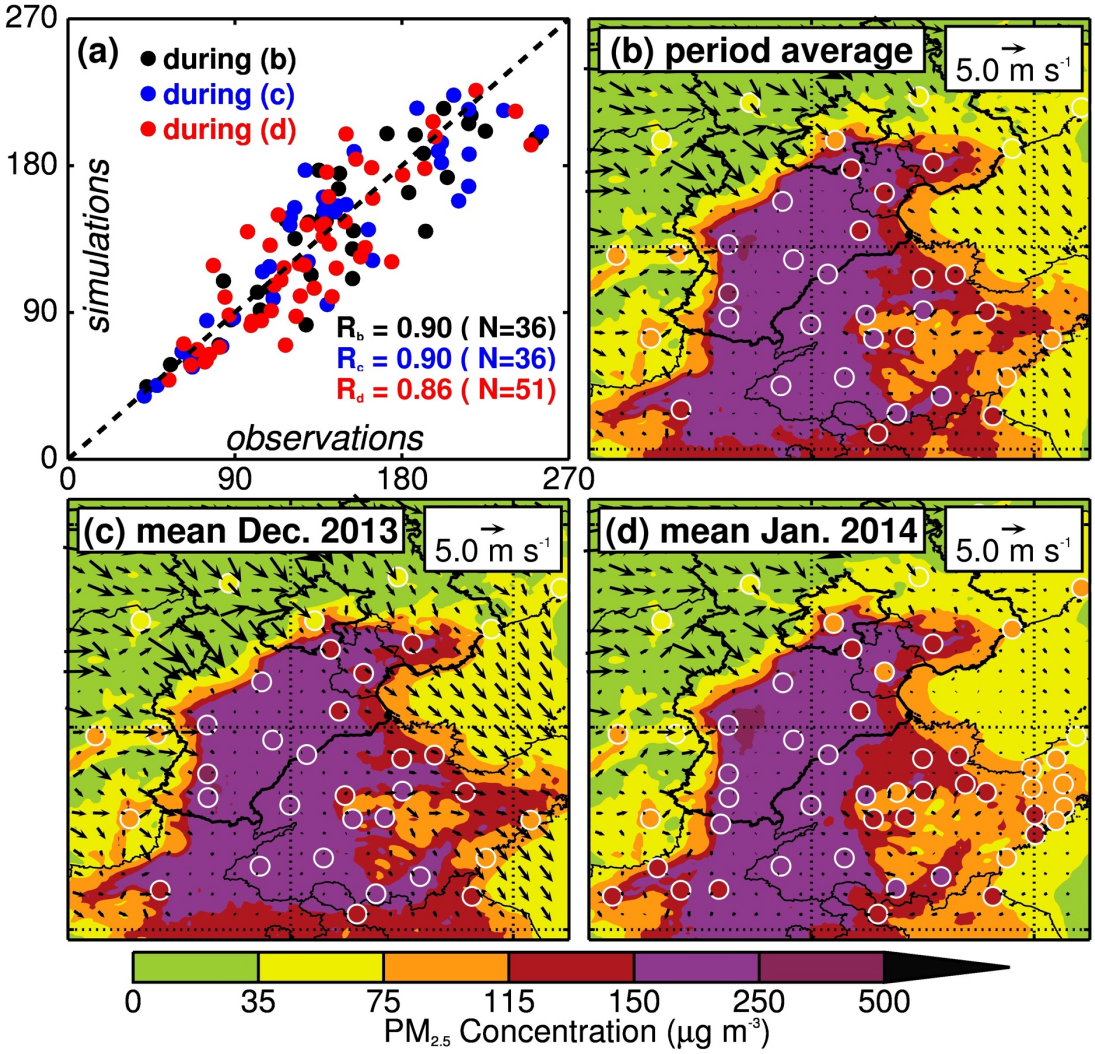

Figure 4 Pattern comparisons of calculated and observed near-surface $PM_{2.5}$ mass concentrations. (a) Spatial correlation between calculated and observed $PM_{2.5}$ concentrations during each month and the whole simulation period. Horizontal distribution of calculated (color contour) and observed (colored circles) average $PM_{2.5}$ concentrations during (b) the whole simulation period, (c) December 2013, and (d) January 2014, along with the simulated wind fields (black arrows).

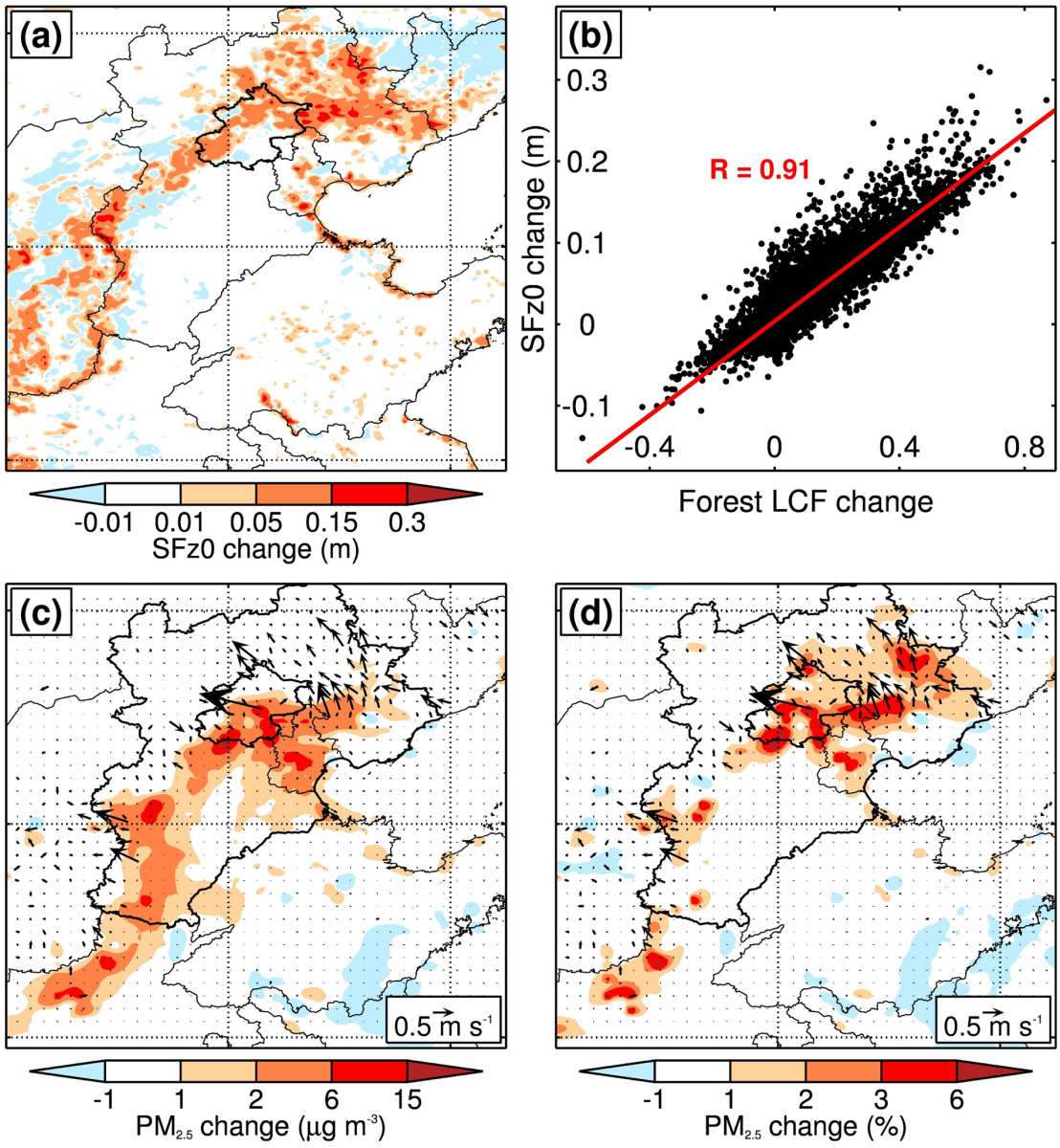

Figure 5 (a) SFz0 change from 2001 to 2013, and (b) its correlation with the forest LCF change; Horizontal distribution of (c) absolute and (d) relative near-surface $PM_{2.5}$ mass concentration changes caused by the afforestation. The wind field changes are shown in black arrows in (c) and (d).

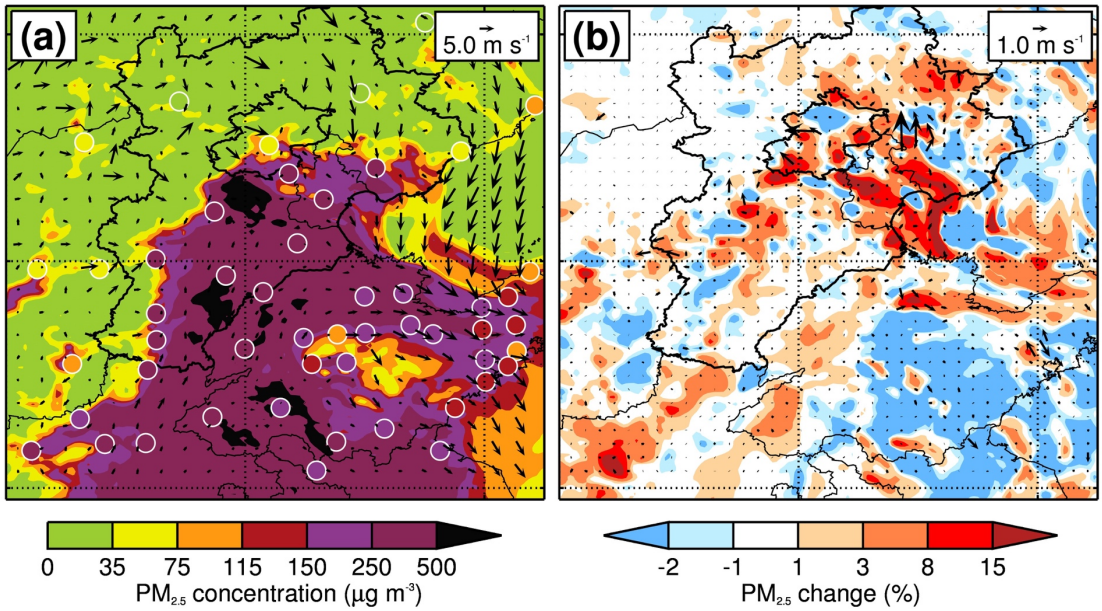

Figure 6 Horizontal distribution of (a) the average near surface $PM_{2.5}$ mass concentration and (b) its change due to the afforestation during an intensified northerly/northwesterly event from 00:00 to 10:00 Beijing Time on January 18, 2014. The wind field and its change are shown in black arrows.

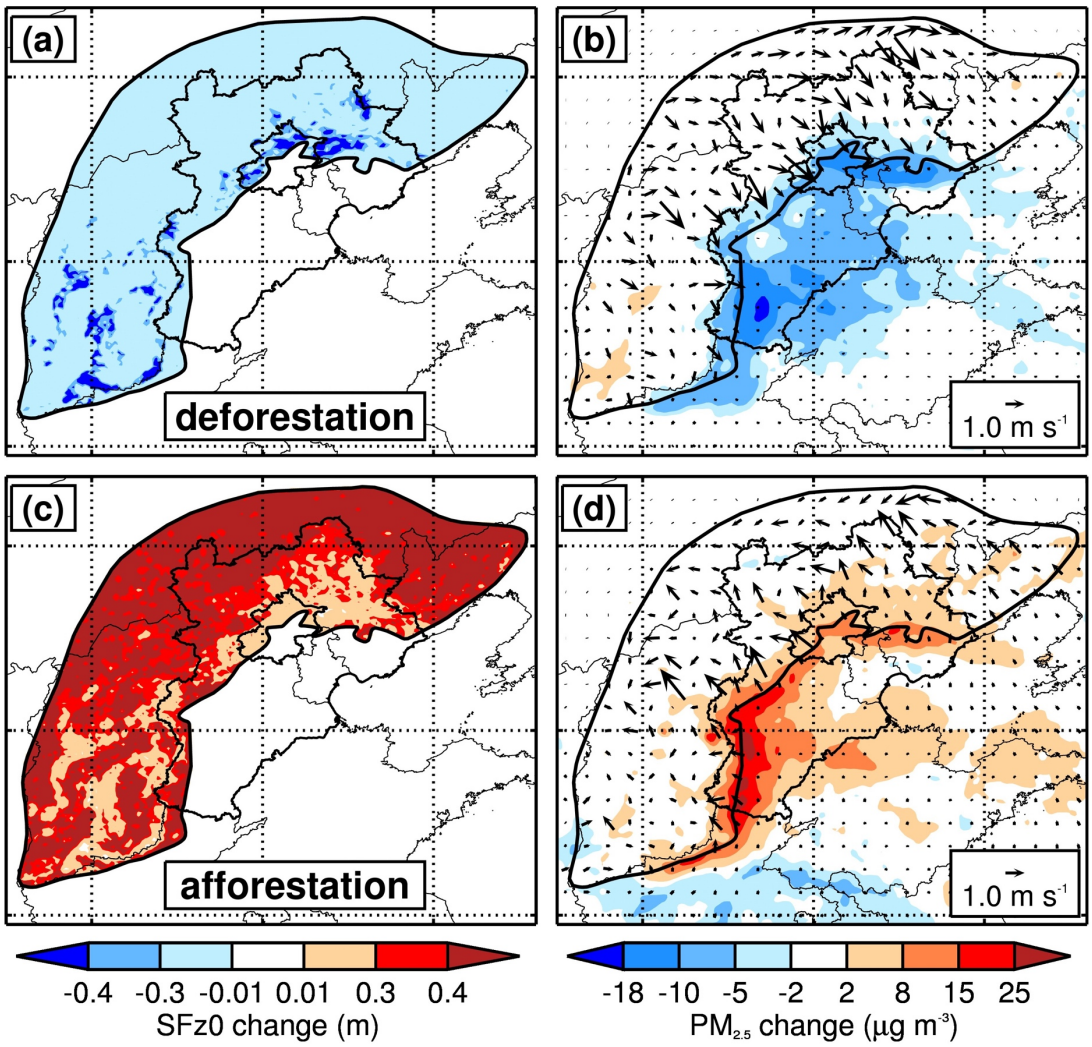

Figure 7 Impacts of complete deforestation/afforestation over Taihang and Yanshan Mountains on (a)/(c) SFz0 and (b)/(d) average near-surface $PM_{2.5}$ mass concentrations from 1 December 2013 to 31 January 2014, along with the wind field change (black arrows).

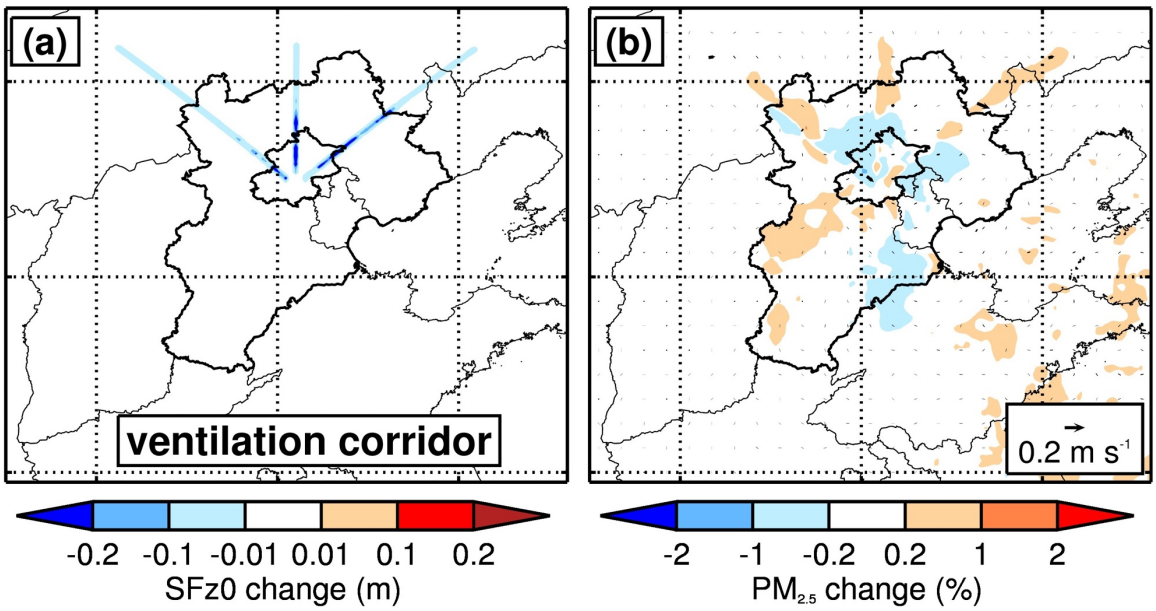

Figure 8 Impacts of an artificial large ventilation corridor system on (a) SFz0 and (b) average near-surface $PM_{2.5}$ mass concentrations from 1 December 2013 to 31 January 2014, along with the wind field (black arrows).